Supporting Information

Kinetic Control in Assembly of Plasmid DNA/Polycation Complex Nanoparticles

Yizong Hu,[†,‡] Zhiyu He,[‡,§] Yue Hao,[¶] Heng-wen Liu,[‡,§] Like Gong,[‡,§] Gregory Howard,[†,‡] Hye-Hyun Ahn,[¤] Mary Brummet,[¤] Xiyu Ke, [‡,§] Caleb Anderson,[‡,#] Jung-Hee Seo,[¶] Jinchang Zhu,[‡,§] Kuntao Chen,[‡,§] Marion Pang Wan Rion,[†,‡] Honggang Cui,[‡,#] Christopher G. Ullman,[^] Christine A. Carrington,[^] Martin G. Pomper,[¤,‡] Rajat Mittal,[¶] Il Minn,[¤,‡] and Hai-Quan Mao*[,†,ǂ,‡,§]

[†]Department of Biomedical Engineering, [¤]Russell H. Morgan Department of Radiology and Radiological Science, and [ǂ]Translational Tissue Engineering Center, Johns Hopkins University School of Medicine, Baltimore, MD 21287, USA.

[‡]Institute for NanoBioTechnology, [§]Department of Materials Science and Engineering, [¶]Department of Mechanical Engineering, and [#]Department of Chemical and Biomolecular Engineering, Johns Hopkins University, Baltimore, MD 21218, USA.

[^]Cancer Targeting Systems, Chesterford Research Park, Cambridge, CB10 1XL, UK.

*Correspondence should be addressed to Dr. Hai-Quan Mao: 3400 N. Charles Street, Croft Hall 100, Institute for NanoBioTechnology, Johns Hopkins University, Baltimore, MD, 21218, USA. Email: hmao@jhu.edu.

Content List of Supporting Information

Supporting Figure S11. Tumor-specific transfection and expression efficiencies of PEC nanoparticles with different *p*DNA payloads and PEI compositions prepared by kinetically controlled conditions in a LL2 lung metastasis model on NSG mice.

Supporting Figure S12. Supplementary biodistribution data of PEC nanoparticle formulations with significant findings in transfection and transgene activities.

Supporting Video S1. Development of velocity isosurface in the CIJ chamber under a flow rate of 20 mL/min.

Supporting Video S2. Development of vorticial structures (Q-criterion vortex isosurface) in the CIJ chamber under a flow rate of 20 mL/min.

Supporting Video S3. Demonstration of the reconstitution process of lyophilized *p*DNA/*in vivo*-jetPEI® nanoparticles.

Table S1. List of plasmid DNAs used in this study

Plasmid	Length	Description
gWiz-Luc	6732 bps	Encodes luciferase protein as a reporter. In this study, serves mainly for the purpose of evaluation of transfection efficiency *in vitro* or *in vivo*.
gWiz-GFP	5757 bps	Encodes GFP protein. In this study, serves only for the purpose of varying plasmid size.
I2	4393 bps	A control plasmid that serves only for the purpose of varying plasmid size.
PEG-Luc	5314 bps	Constructed with PEG-3 promoter, thus providing tumor-specific transfection and expression of luciferase protein as a reporter.

Table S2. Procedures to prepare PEC nanoparticles by pipetting

Procedure	Description
B1	Slow (2 sec) addition of 50 μL PEI working solution on top of 50 μL DNA working solution, immediately following vortex for 30 sec; and 5 min of stabilization applied.
B2	Fast injection of 50 μL PEI working solution into 50 μL DNA working solution, immediately following vortex for 30 sec; and 5 min of stabilization applied.
B3	Fast injection of 100 μL PEI working solution into 100 μL DNA working solution, immediately following vortex for 30 sec; and 5 min of stabilization applied.
B4	Fast injection of 50 μL DNA working solution into 50 μL PEI working solution, immediately following vortex for 30 sec; and 5 min of stabilization applied.

Table S3. Examinations of form factors for static light scattering (SLS) experiments

Plasmid	Input pDNA Concn. (μg/mL)	Input N/P Ratio	Radius of Gyration R_g (nm)	Maximum Form Factor
I2	25	4	12.6	0.310
	50	4	14.7	0.359
	100	4	19.5	0.477
	200	4	27.5	0.674
	400	4	46.8	1.147
gWiz-GFP	25	4	14.2	0.349
	50	4	14.6	0.357
	100	4	18.9	0.463
	200	4	32.5	0.796
	400	4	42.3	1.037
gWiz-Luc	25	4	15.1	0.370
	50	4	17.6	0.430
	100	4	24.7	0.605
	200	3	44.5	1.091
	200	4	35.8	0.877
	200	5	33.4	0.818
	200	6	35.1	0.860
	400	4	75.2	1.842

Accurate radius of gyration R_g results can be obtained regardless of possibly different morphology of the PECs if the experiments are designed with the form factor smaller than 1, such that:

$$qR_g = \frac{4\pi n}{\lambda}\sin\left(\frac{\theta}{2}\right)R_g \leq 1$$

where q is magnitude of scattering vector, R_g is the radius of gyration measured, n is the refractive index of the test solvent (1.333, water), λ is the wavelength of the incident laser beam (658 nm), and θ is the angle of the scattered light. For all PECs prepared with $\tau_M < \tau_A$, the maximum form

factor is obtained with $\theta = 150°$ (largest angle among the detectors) for each formulation and shown in the table.

Most of the formulations have a maximum form factor smaller than 1. For these groups, the radius of gyration was determined directly. For the groups labeled in red, though the maximum form factor is larger than 1, but most of the form factors with lower scattering angles are below 1. Therefore, when determining the radius of gyration for these groups, data points at high scattering angels were not used. In general, all the radius of gyration values reported in this study can disregard the specific morphology of the PEC nanoparticles.

Table S4. Summary of the characteristics of the nanoparticles with different weight average copy numbers of *p*DNA per nanoparticle ($\overline{N}$) tested *in vitro* and *in vivo*

FNC input *p*DNA Concentration	$\overline{N}$	Z-Average Hydrodynamic Size* (nm)	Zeta-potential* (mV)	Bound PEI Percentage (%)	Free PEI per μg *p*DNA dose (μM)
100	1.7	49.4 ± 18.5	+42.3 ± 1.5	73.1 ± 0.7	3.24 ± 0.08
200	3.5	63.4 ± 23.7	+41.1 ± 1.8	69.1 ± 1.2	3.64 ± 0.12
400	6.1	81.2 ± 32.7	+41.6 ± 1.8	69.7 ± 2.6	3.63 ± 0.32
800	21.8	132.1 ± 53.0	+39.7 ± 0.7	67.2 ± 2.1	3.94 ± 0.26

* Reported as Z-average hydrodynamic diameter ± DLS size standard deviation.

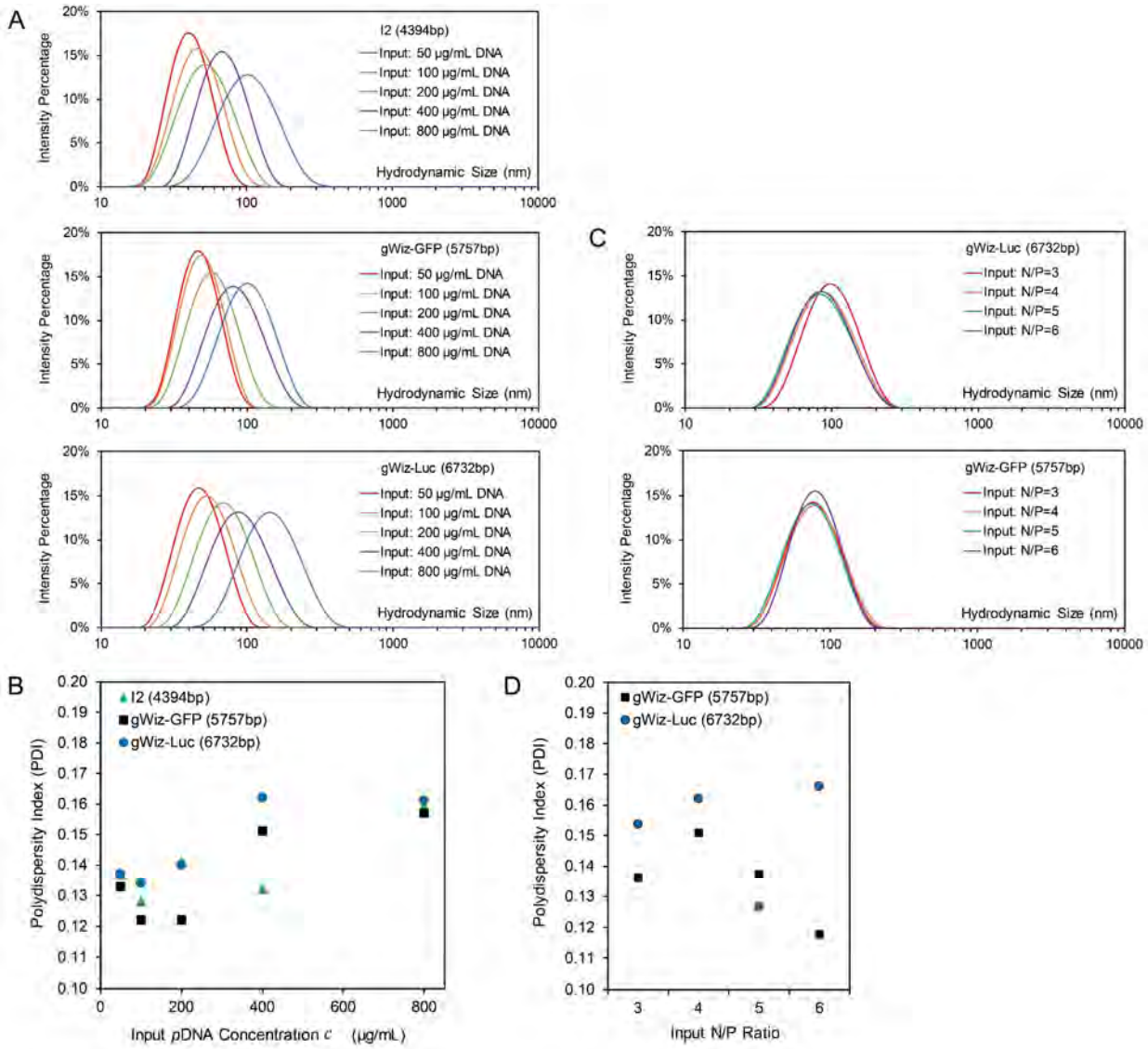

Figure S1. Size distributions of PEC nanoparticles formulated with different input *p*DNA concentrations and input N/P ratios with $\tau_M < \tau_A$. (A) Size distributions and **(B)** polydispersity index (PDI) of nanoparticles prepared by different input *p*DNA concentrations; **(A)** Size distributions and **(B)** polydispersity index (PDI) of nanoparticles prepared by different input N/P ratios.

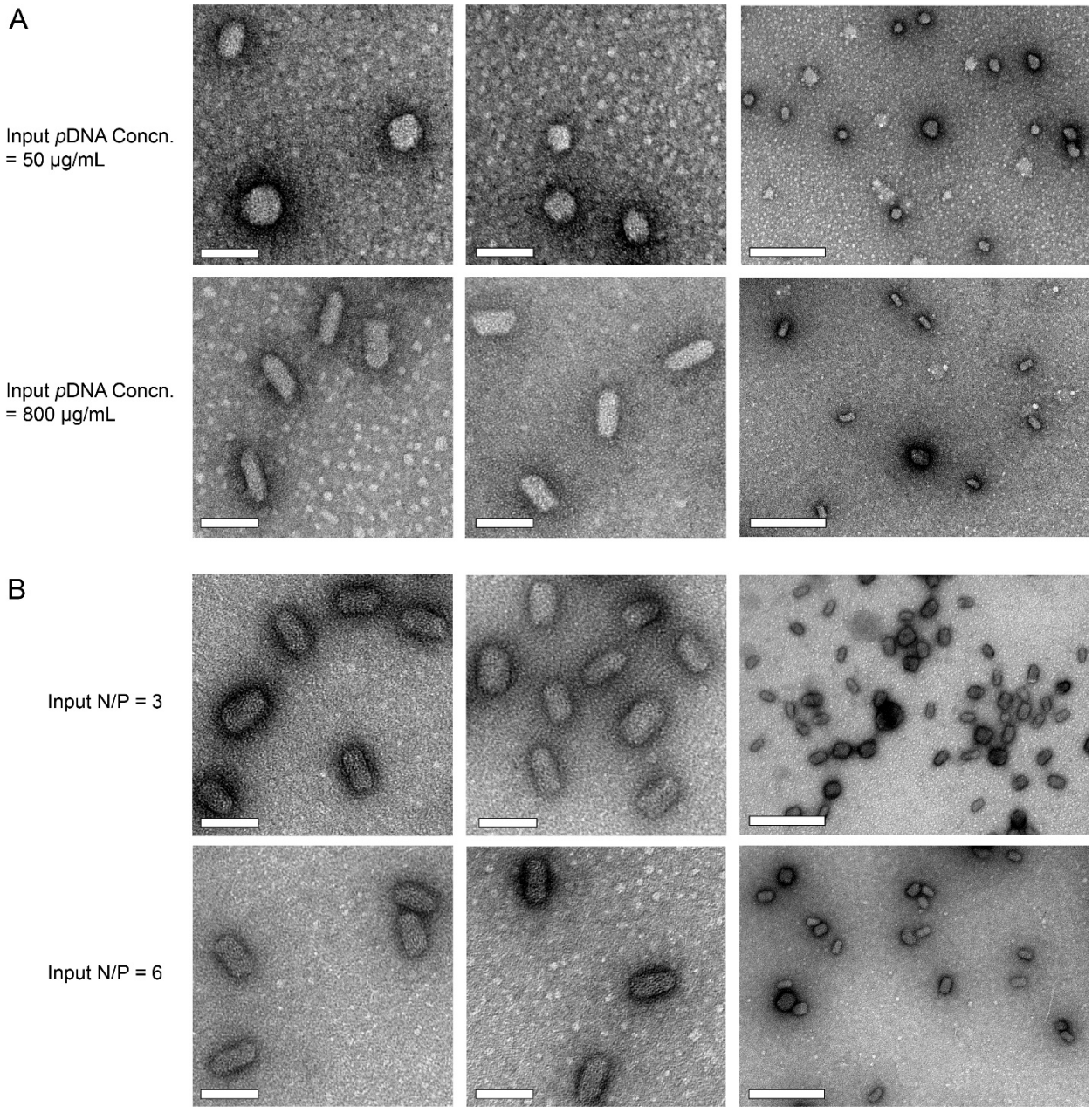

Figure S2. Supplementary TEM images for nanoparticles prepared by different input *p*DNA concentrations and N/P ratios. TEM images of **(A)** gWiz-Luc PEC nanoparticles prepared with an input *p*DNA concentration of 50 and 800 µg/mL. Note that the TEM images of gWiz-Luc PEC nanoparticles prepared with an input *p*DNA concentration of 200 µg/mL are shown in **Fig. 2C**. These TEM observations show the uniformity of the *p*DNA/*in vivo*-jetPEI® nanoparticles prepared under turbulent mixing conditions at impinging flow rate of Q = 20 mL/min; **(B)** gWiz-GFP PEC nanoparticles prepared with input N/P ratio of 3 or 6, demonstrating similarity of size across preparations with different N/P ratios. Scale bar = 50 nm (for left two panels) and 200 nm (for right panel).

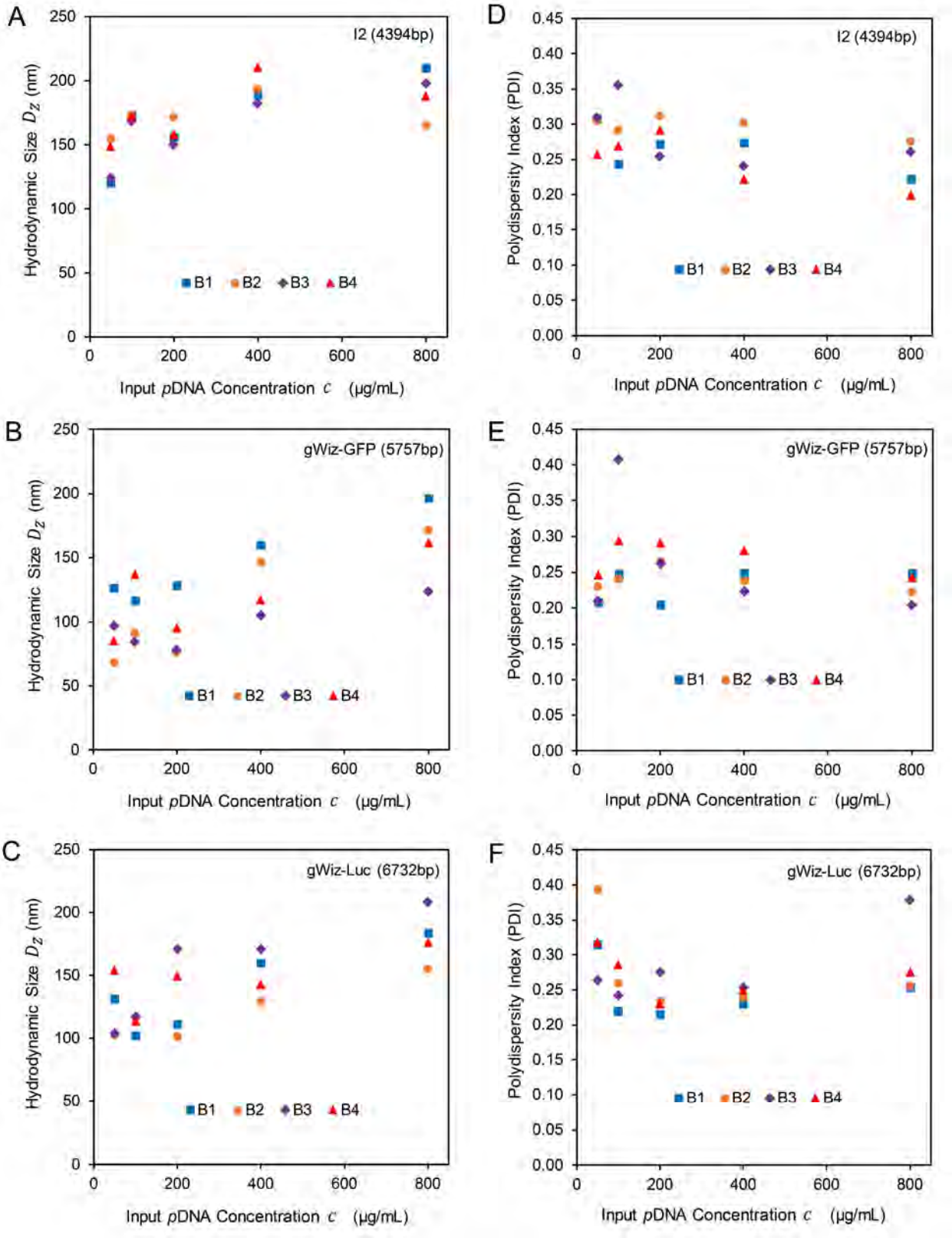

Figure S3. Non-uniform PEC nanoparticles produced by pipetting method without tunability of size by input *p*DNA concentrations. | The size of the PEC nanoparticles made by **(A)** I2 plasmid; **(B)** gWiz-

GFP plasmid; **(C)** gWiz-Luc plasmid; and polydispersity index (PDI) of PEC nanoparticles made from **(D)** I2 plasmid; **(E)** gWiz-GFP plasmid; **(F)** gWiz-Luc plasmid. Labels: B1, B2, B3 and B4 represent 4 different procedures followed to make nanoparticles by pipetting, see **Table S2**.

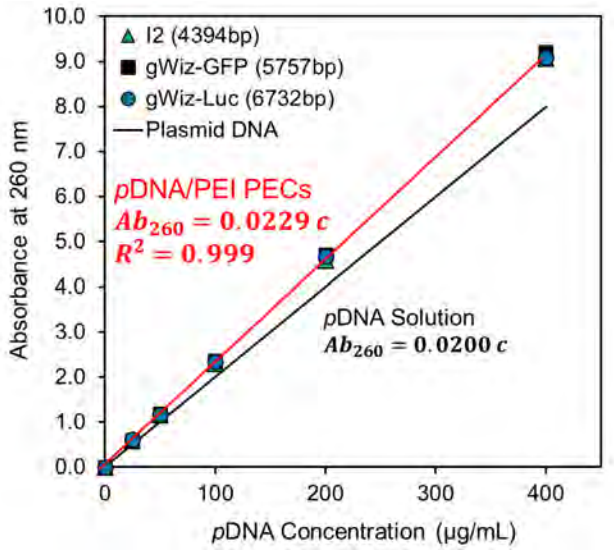

Figure S4. Determination of *p*DNA concentration in PEC nanoparticle suspensions. Upon PEI binding and assembly, the absorbance at 260 nm by *p*DNA molecules increases but still follow a linear relationship with respect to *p*DNA concentrations. This standard curve was used to assess *p*DNA concentrations in any PEC nanoparticle suspensions.

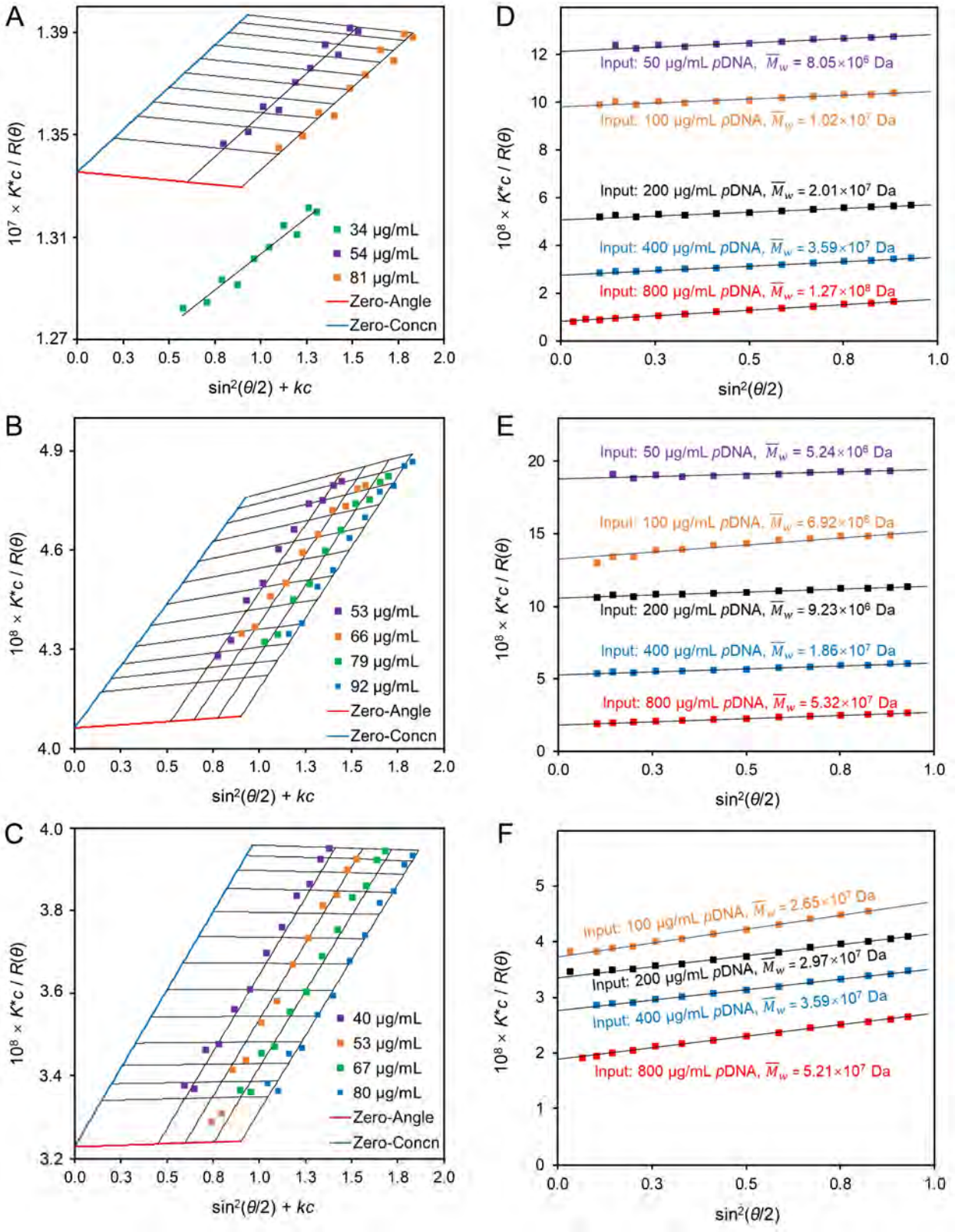

Figure S5. Supplementary SLS data for nanoparticles prepared by a flow rate of 20 mL/min with different input *p*DNA concentrations and N/P ratios. | Full Zimm plots of gWiz-Luc PEC nanoparticles

with **(A)** a molar mass of 1.02×10^7 Da, and 1.7 *p*DNAs per nanoparticle; **(B)** a molar mass of 3.59×10^7 Da, and 6.1 *p*DNAs per nanoparticle; **(C)** a molar mass of 1.27×10^8 Da, and 21.8 *p*DNAs per nanoparticle, demonstrating a universal zero second virial coefficient; Combined Debye plots for PEC nanoparticles prepared with different input *p*DNA concentrations by **(D)** I2 plasmid and **(E)** gWiz-Luc plasmid; or **(F)** different input N/P ratios by gWiz-Luc plasmid.

For **(A)**, the original 34 μg/mL (total mass concentration in nanoparticle) sample was concentrated to 81 μg/mL and then diluted to have 54 μg/mL. The molar mass seemed to have had decreased slightly upon concentration by filtration. But overall, the 81 μg/mL and 54 μg/mL data points suggested that the system presented a second virial coefficient that is equal to 0.

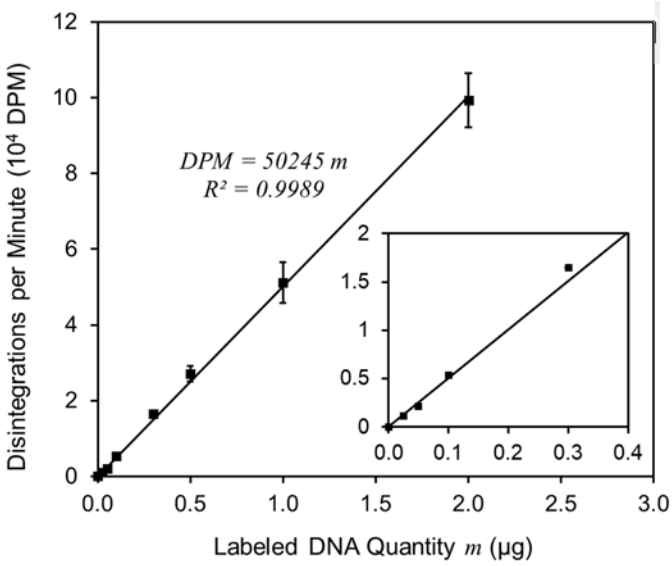

Figure S6. Standard curve for quantitative assessment of absolute amount of ^{3}H-labeled *p*DNA in biological samples. Different amount of ^{3}H-labeled *p*DNA solutions were added into 4 mL scintillation fluid contained in 7-mL glass scintillation vials. The same readings procedures were applied as described in the **Experimental Section** to obtain the standard curve. All readings of real biological samples (cell lysate or mouse tissue solute) fell into the quantity range shown in this standard curve.

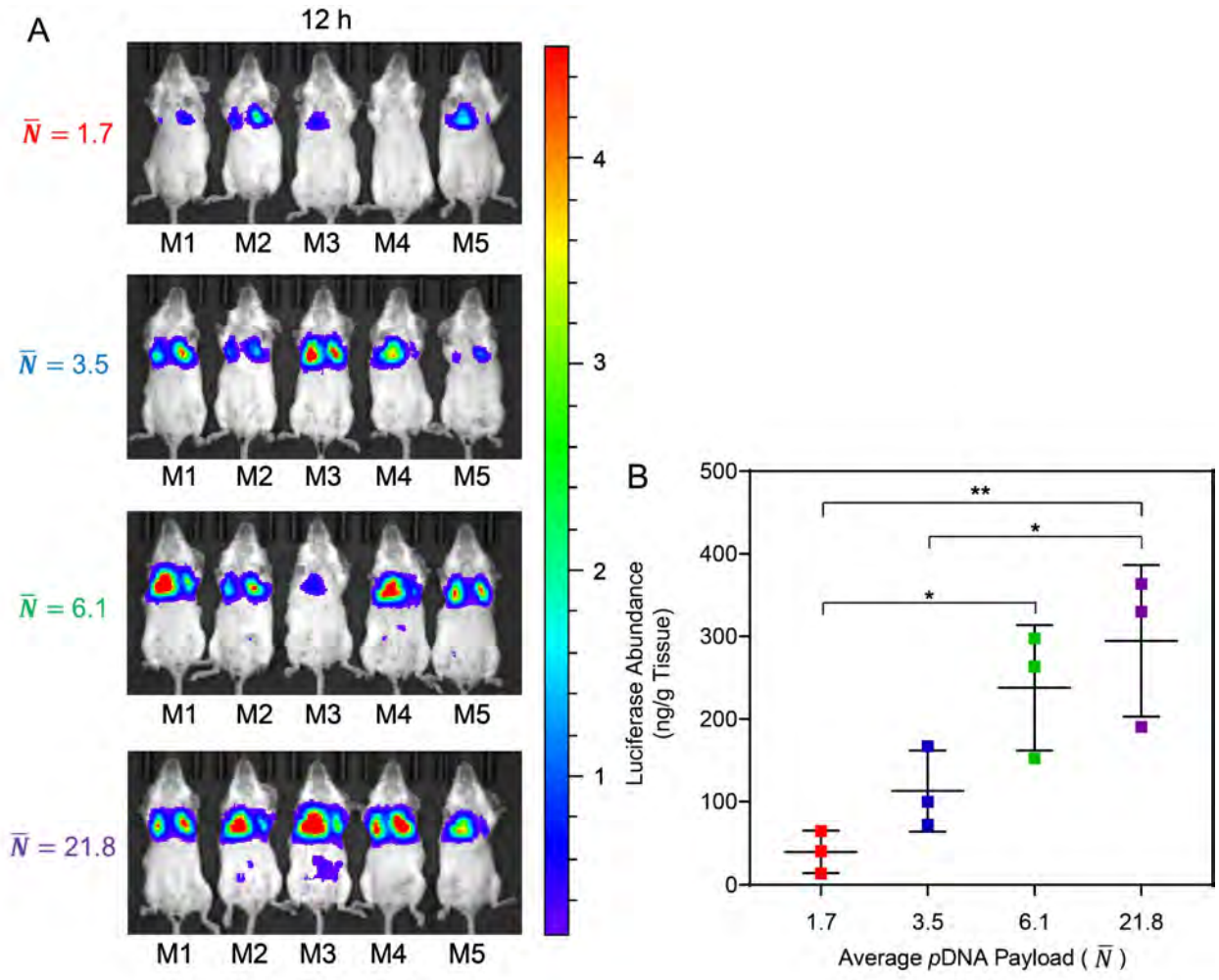

Figure S7. ***In vivo*** **transfection efficiency in lungs upon dosing of PEC nanoparticles with different weight average copy numbers of *p*DNA per nanoparticle ($\overline{N}$). (A)** IVIS whole-body bioluminescence images of all groups at 12-h post injection of nanoparticles containing 30 μg *p*DNA per mouse. Scale bar: local radiance with unit of 10^6 photon/s/cm^2/sr; **(B)** Luciferase abundance as measured in homogenized lungs in 3 mice with highest signals, showing a perceived trend that PEC nanoparticles with a higher *N* gave better transfection efficiency in lungs.

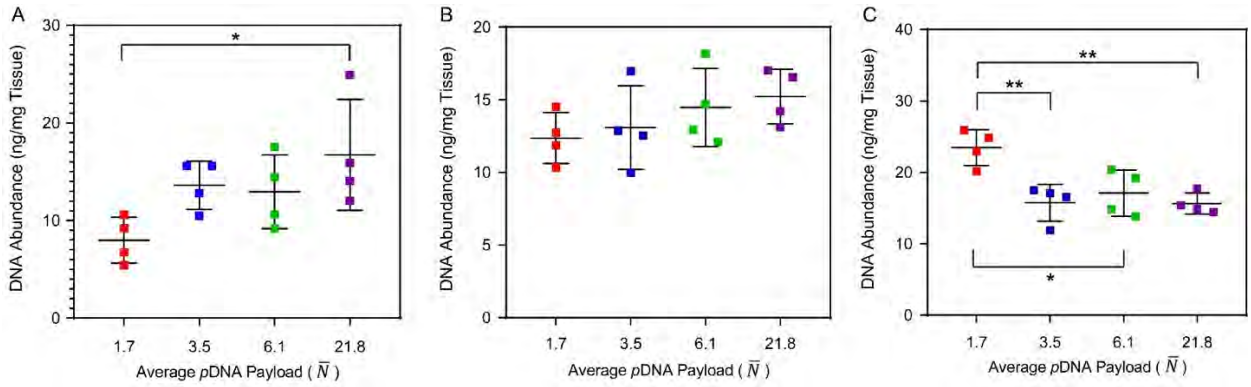

Figure S8. Biodistribution of dosed PEC nanoparticles with different weight average copy numbers of *p*DNA per nanoparticle ($\bar{N}$). The abundance of delivered *p*DNA in **(A)** lungs; **(B)** liver; and **(C)** spleen.

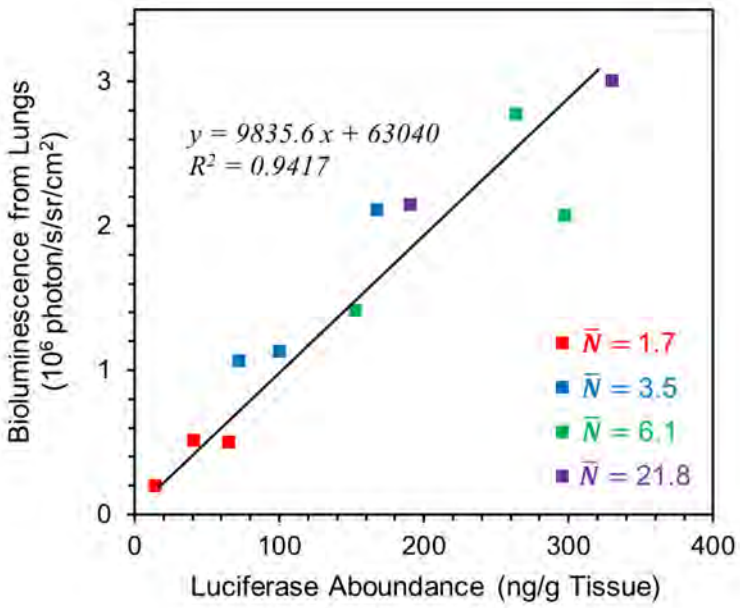

Figure S9. Correlation between IVIS region of interest (ROI) quantitative results and luciferase abundance in tissue. The IVIS ROI quantitative analysis was done with an exposure time of 30 seconds to the lung area with mice dosed with PEC nanoparticles with different $\bar{N}$ as shown in **Fig. S7**. The lungs were harvested from the mice immediately after the imaging and were homogenized in luciferase assay report lysis buffer (Promega, US) by a sonication probe to release the luciferase protein. Then the luciferase quantity in the tissue sample was determined as described in **Experimental Section** for *in vitro* transfection efficiency assessment.

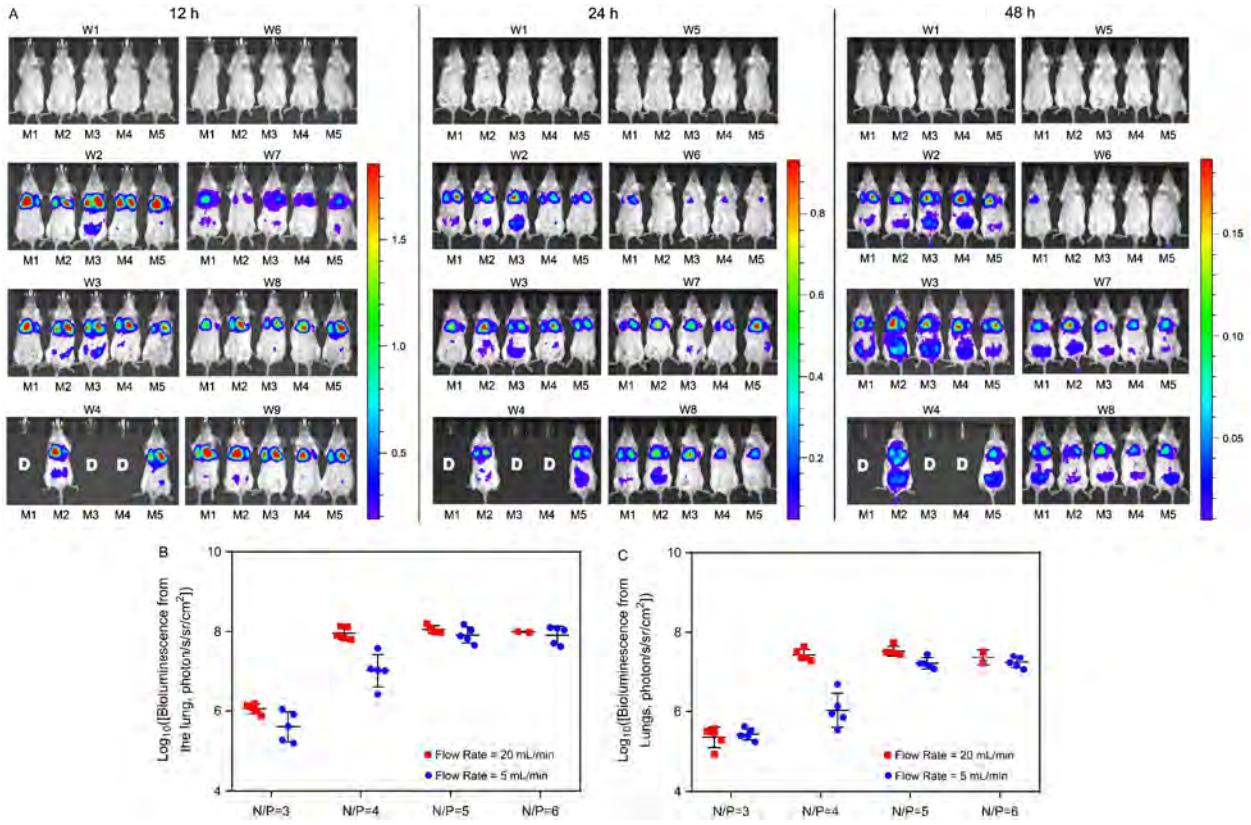

Figure S10. ***In vivo*** **transfection efficiencies of PEC nanoparticles with different *p*DNA payloads and PEI compositions prepared by kinetically controlled conditions in healthy BALB/c mice. (A)** IVIS whole-body images of all groups dosed with formulations listed in **Table 1** at 12, 24 and 48-h post injection of PEC nanoparticles containing 40 μg *p*DNA per mouse. The label **D** denotes died mouse due to toxicity; Scale bar: local radiance with unit of 10^7 photon/s/cm^2/sr; and the IVIS ROI quantitative analysis results at **(B)** 24 and **(C)** 48-h post-injection.

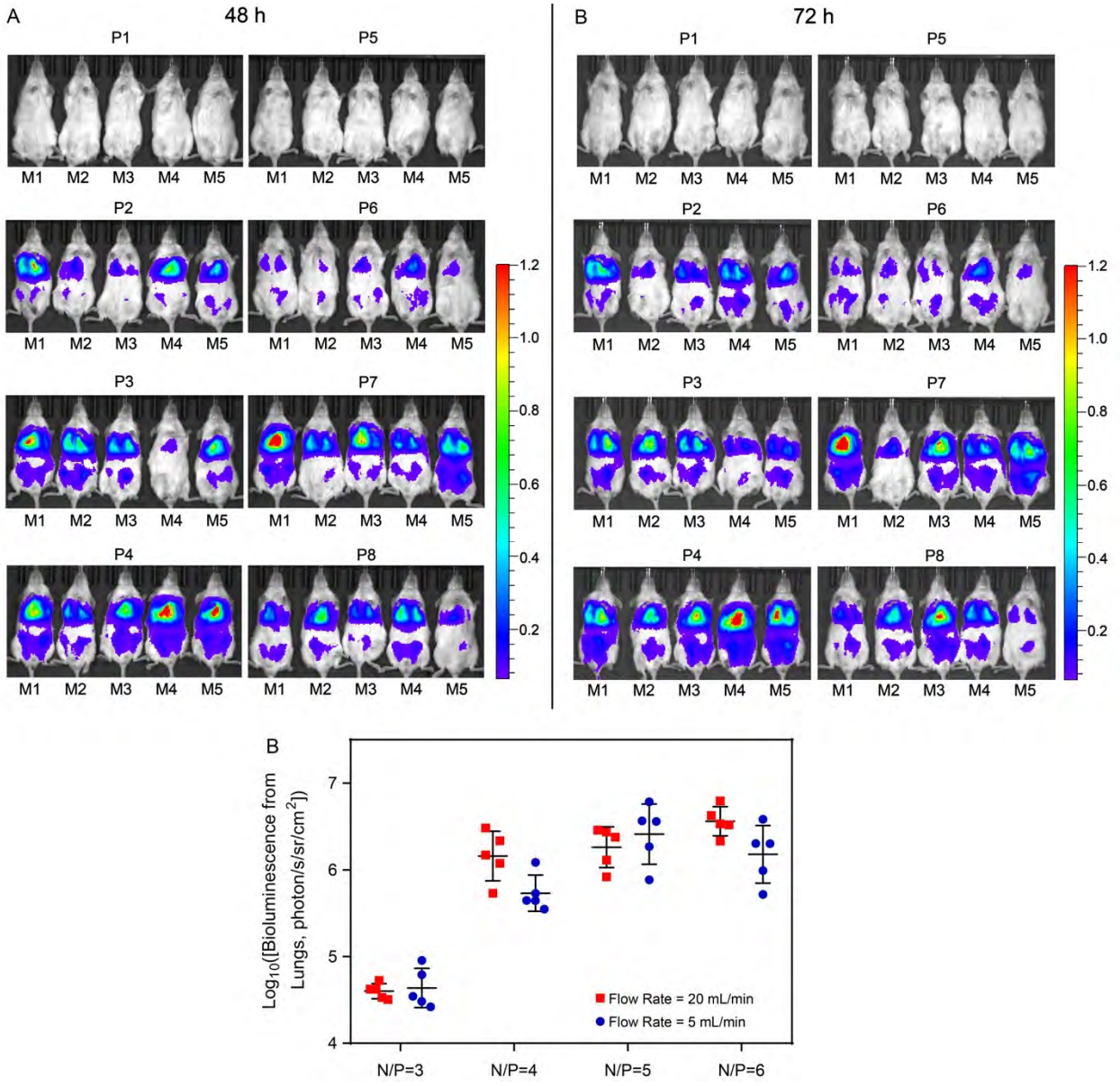

Figure S11. Tumor-specific transfection and expression efficiencies of PEC nanoparticles with different *p*DNA payloads and PEI compositions prepared by kinetically controlled conditions in a LL2 lung metastasis model on NSG mice. (A) IVIS whole-body images of all groups dosed with formulations listed in **Table 1** at 48 and 72-h post injection of PEC nanoparticles containing 40 μg *p*DNA per mouse. Scale bars: local radiance with unit of 10^6 photon/s/cm^2/sr; **(B)** IVIS ROI quantitative analysis results at 72-h post-injection time point.

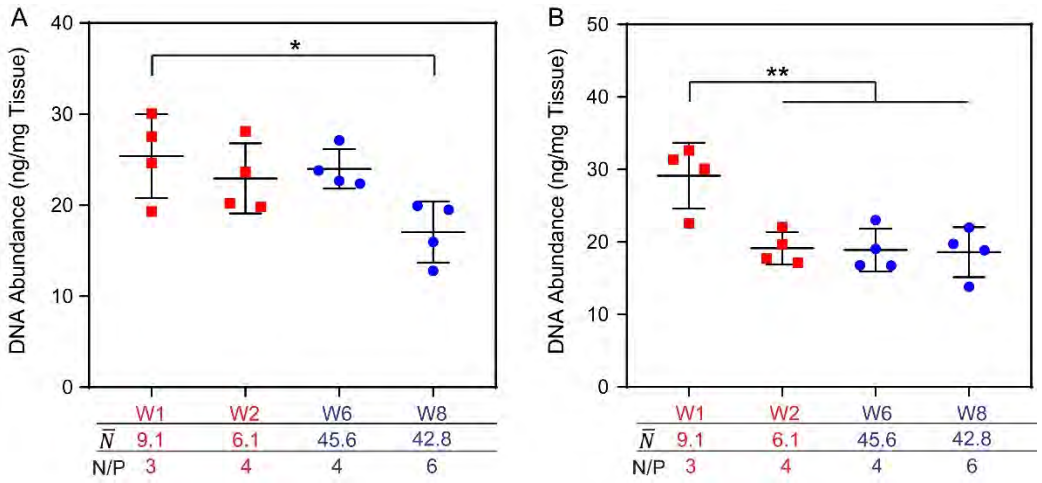

Figure. S12. Supplementary biodistribution data of PEC nanoparticle formulations with significant findings in transfection and transgene activities. (A) *p*DNA abundance in liver; **(B)** *p*DNA abundance in spleen.